One-dimensional nonlocal elasticity for tensile single-walled carbon nanotubes: A molecular structural mechanics characterization

M. Malagù[a,b,*], E. Benvenuti[a], A. Simone[b]

[a] *Engineering Department, University of Ferrara, Via Saragat 1, 44122 Ferrara, Italy*
[b] *Faculty of Civil Engineering and Geosciences, Delft University of Technology, P.O. Box 5048, 2600 GA Delft, The Netherlands*

Abstract

The parameters required for modeling tensile single-walled carbon nanotubes (SWCNTs) with a nonlocal rod model are estimated. Molecular structural mechanics (MSM) simulations are carried out for the mechanical analysis of SWCNTs with different diameter, length and chirality. Representative axial strain fields are then used in a parameter estimation procedure as reference solutions to tailor a nonlocal rod model. Obtained nonlocal parameters are further validated by comparing the total strain energy of MSM reference solutions and corresponding nonlocal rod solutions. The effect of size and chirality on the optimal value of the estimated parameters is discussed in details. Analytical relations between nonlocal parameters and geometry of the SWCNTs are obtained.

Keywords: single-walled carbon nanotubes, molecular structural mechanics, nonlocal elasticity, parameter estimation

1. Introduction

Fundamental insight into the behavior of carbon nanotubes (CNTs) is customarily obtained with atomistic simulations [1]. Although accurate, these simulations are usually computationally intensive and not particularly suited for the analysis of long CNTs or more complex systems such as CNT networks or composites. Here, we propose a one-dimensional nonlocal rod model which is kinematically and energetically equivalent to a generic axially loaded single-walled carbon nanotube (SWCNT).

The most used atomistic approaches for the analysis of carbon nanotubes (CNTs) include *ab initio* calculations [2], molecular dynamics [3], and molecular mechanics [4]. Although accurate, the application of these procedures is limited to small-scale atomistic systems. In an effort to decrease the computational effort of atomistic simulations, Li and Chou [5] proposed a simple and efficient approach, referred to as molecular structural mechanics (MSM), which combines molecular mechanics and classical structural mechanics. In MSM, CNTs are modeled as space

*Corresponding author
Email addresses: mlgmcl@unife.it (M. Malagù), bnvlne@unife.it (E. Benvenuti), a.simone@tudelft.nl (A. Simone)

frame structures in which beam and spring elements replace covalent bonds between carbon atoms. Based on this concept, Tserpes and Papanikos [6] developed a three-dimensional finite element model to investigate the mechanical properties of armchair, zigzag and chiral SWCNTs. The results obtained by these authors are in good agreement with those provided by theoretical and experimental studies [7–9]. The computational effort of MSM is, however, still considerable for long nanotubes.

An alternative approach to atomistic simulations of CNTs relies on equivalent continuum formulations which are relatively simpler and result in a reduced computational effort. In modeling SWCNTs with a continuum mechanics model, the discrete atomic lattice of the nanotube is replaced by a continuous and homogeneous solid. In general, either isotropic and anisotropic shells [7, 10] or one-dimensional theories such as Euler-Bernoulli and Timoshenko beam models [11, 12] as well as rod models [13] are employed.

The use of classical continuum formulations at the nanoscale, however, might be questionable [14]. Classical theories do not account for small length scale effects induced by the discrete structure of SWCNTs. Promising approaches are those based on nonlocal continuum mechanics which allows the consideration of size effects by introducing small-scale parameters in the constitutive relation. The main advantage of a nonlocal formulation lies on the possibility of accounting for interatomic long range interactions (in Eringen's nonlocal theory [15], the strain at a given point is a weighted average of the strain at surrounding points). Applications of nonlocal continuum mechanics to the study of CNTs are reported in several papers [16–18].

Although several studies on the modeling of SWCNTs with nonlocal formulations have been carried out, only few attempts have been made to determine the value of the nonlocal parameters. Duan et al. [19] and Hu et al. [20] calibrated the small-scale parameters for the free vibration problem in SWCNTs by using molecular dynamics simulations. They found that the estimated nonlocal parameters vary with the aspect ratio, mode shapes and boundary conditions of the SWCNTs. A similar approach was used in [21] to capture size effects in the dynamic torsional response of $(6,6)$ and $(10,10)$ armchair SWCNTs with a nonlocal shell model. Naredar et al. [22], by using MSM, derived an expression of the small scale parameters to study the ultrasonic wave propagations in SWCNTs.

In this contribution, we estimate the nonlocal parameters for tensile armchair, zigzag and chiral SWCNTs by comparing the axial strain field calculated with MSM and a nonlocal elastic rod model. First, MSM is used to investigate size and chirality effects on SWCNTs Young's modulus and on the strain field in tensile simulations as discussed in Section 2.3 and 2.4, respectively. Then, a two-component local/nonlocal model [23, 24], a variant of the classical integro-differential Eringen's formulation, is considered for the modeling of SWCNTs as continuum rods. The corresponding one-dimensional constitutive equation is summarized in Section 3. Instead of the classical Gaussian kernel, the atomistically-based kernel developed by Picu [25] is adopted. As in atomic pair potentials [26],

this kernel has a positive value at the origin and becomes negative at some distance. Finally, the identification of the nonlocal parameters is performed by means of an optimization procedure by minimizing the discrepancy between MSM and nonlocal axial strain fields as described in Section 4. To improve the agreement between atomistic and nonlocal results, the quadratic penalty method [27] is used. The effect of diameter and chirality on the value of the calculated parameters is further discussed. Hence, an analytical relation between the nonlocal parameters and the nanotubes diameter and chirality is derived.

To our knowledge, this paper represents a first attempt to estimate nonlocal parameters for the modeling of SWCNTs subjected to static axial load by using an atomistic (MSM) model. The results presented herein ensure the reliability of nonlocal formulations to model tensile carbon nanotubes and, in particular, to predict their axial strain field and strain energy.

2. Molecular structural mechanic simulations of single-walled carbon nanotubes

2.1. Atomic model of single-walled carbon nanotubes

Molecular structural mechanics (MSM) is an atomistic modeling technique to study the mechanical properties of materials at the atomic scale. Similar to molecular mechanics (MM), molecules in MSM are modeled as discrete systems of balls (representing atoms) and springs (representing covalent and non-covalent bonds). Thus, knowing the position of the atoms and the stiffness of the chemical bonds that hold them together allows to predict the mechanical response of an atomic structure.

The constitutive equations for the structural elements depend on the mathematical relations describing the total potential energy Π of a molecule [28] which is expressed as:

$$\Pi = \sum_{bonds} \Pi_{stretch}(\Delta r) + \sum_{angles} \Pi_{bend}(\Delta\omega) + \sum_{dihedrals} \Pi_{torsion}(\Delta\phi) + \sum_{pairs} \Pi_{nonbond}(\Delta r). \tag{1}$$

Here, $\Pi_{stretch}$, Π_{bend}, $\Pi_{torsion}$ and $\Pi_{nonbond}$ are the energy contributions corresponding to bond stretching, angle bending, torsional motion around a single bond and stretching of non-covalent bonds (van der Waals forces), while Δr, $\Delta\omega$ and $\Delta\phi$ denote variations of covalent or non-covalent bonds length and angles between three atoms and dihedral angles (see Figure 1 for a representation of these quantities). As observed in Refs. [5, 29], the energy contribution from van der Walls interactions is negligible for covalent systems undergoing small deformations. Therefore, we neglect the contribution of $\Pi_{nonbond}$ in (1) since the small deformation hypothesis is adopted in this work.

Assuming the bond stretching and angle bending terms defined by the modified Morse potential [4] and the tor-

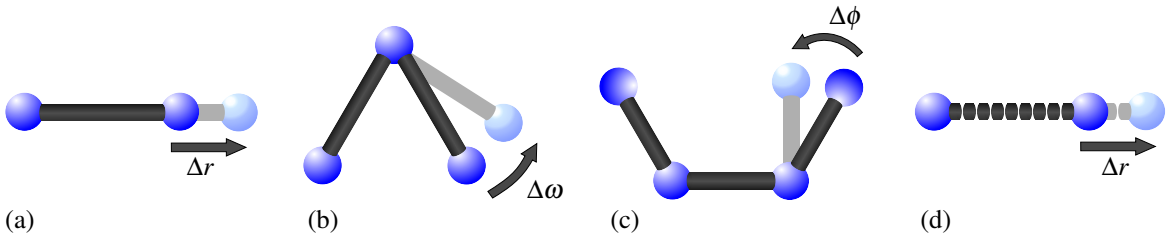

Figure 1: Interatomic interactions in molecular structural mechanics: (a) bonds stretching, (b) angle bending, (c) torsion and (d) stretching of non-covalent bonds.

sional contribution described by a parabolic function [30], the energy contributions in (1) are defined as:

$$\Pi_{stretch}\left(\Delta r\right) = D_e\left[\left(1-\mathrm{e}^{-\beta\Delta r}\right)^2 - 1\right], \tag{2}$$

$$\Pi_{bend}\left(\Delta\omega\right) = \frac{k_\omega}{2}\Delta\omega^2\left[1+k_{sextic}\Delta\omega^4\right], \text{ and} \tag{3}$$

$$\Pi_{torsion}\left(\Delta\phi\right) = \frac{k_\phi}{2}\Delta\phi^2. \tag{4}$$

According to Refs. [4, 30], the constant parameters D_e, β, k_ω, k_{sextic} and k_ϕ are equal to 0.603105 nN nm, 26.25 nm^{-1}, 0.9 nN nm/rad^2, 0.754 rad^{-4}, and 0.278 nN nm/rad^2, respectively.

To study the mechanical properties of SWCNTs with MSM, we consider a frame finite element model geometry computed according to Ref. [31] with the constitutive equations of each structural element derived from (2)–(4). More specifically, the covalent bonds are defined as two-node space frame elements with the relation between axial force and axial stretch expressed as

$$F\left(\Delta r\right) = \frac{\mathrm{d}\Pi_{stretch}\left(\Delta r\right)}{\mathrm{d}\Delta r} = 2\beta D_e\left(1-\mathrm{e}^{-\beta\Delta r}\right)\mathrm{e}^{-\beta\Delta r}. \tag{5}$$

Since the C–C bonds remain straight during deformation, we assume corresponding flexural and torsional stiffness values such that bending and torsional deformations are negligible when compared to the axial strains. Bending and torsional terms are modeled by means of torsional spring elements. Hence, according to (3) and (4), the constitutive

equations between moments and angle variations are defined as

$$M_b\left(\Delta\omega\right) = \frac{\mathrm{d}\Pi_{angle}\left(\Delta\omega\right)}{\mathrm{d}\Delta\omega} = k_\omega \Delta\omega\left(1 + 3k_{sextic}\Delta\omega^4\right) \qquad \text{and} \qquad M_t\left(\Delta\phi\right) = \frac{\mathrm{d}\Pi_{torsion}\left(\Delta\phi\right)}{\mathrm{d}\Delta\phi} = k_\phi \Delta\phi. \tag{6}$$

2.2. Model geometry

The geometry of the model in the MSM simulations is built with reference to the atomic structure of the nanotubes. SWCNTs are periodic cylindrical cage-like structures of carbon atoms with high aspect ratio and diameter in the nanoscale range. The cylindrical shape consists of a mono layer graphene sheet. Geometric and mechanical properties of SWCNTs depends on the rolling angle, that is the orientation of the carbon lattice with respect to the longitudinal axis of the nanotube.

The geometric properties of a single-walled carbon nanotube are usually expressed in terms of diameter d, chiral angle θ, and length L. With reference to Figure 2(a), and denoting the distance of the carbon-carbon bonds with a_{cc} (here assumed equal to 0.1421 nm), diameter and chirality are uniquely defined by the chiral vector

$$\mathbf{C}_h = n_1\mathbf{a_1} + n_2\mathbf{a}_2 \tag{7}$$

in which n_1 and n_2 are a couple of integers, and $\mathbf{a}_1$ and $\mathbf{a}_2$ the basis vectors

$$\mathbf{a}_1 = \left(\frac{\sqrt{3}}{2}, \frac{1}{2}\right)\sqrt{3}a_{cc} \qquad \text{and} \qquad \mathbf{a}_2 = \left(\frac{\sqrt{3}}{2}, -\frac{1}{2}\right)\sqrt{3}a_{cc}. \tag{8}$$

The length of $\mathbf{C}_h$ specifies the circumference C of the nanotube. Therefore, the diameter of an SWCNT can be calculated as

$$d = \frac{C}{\pi} = \frac{a_{cc}\sqrt{3\left(n_2^2 + n_1^2 + n_1 n_2\right)}}{\pi}. \tag{9}$$

The angle between $\mathbf{C}_h$ and the basis vector $\mathbf{a}_1$ denotes the chiral angle

$$\theta = \arctan\left(\frac{\sqrt{3}n_2}{2n_1 + n_2}\right). \tag{10}$$

Carbon nanotubes are named after the value assumed by the chiral angle θ. If $\theta = 0$, $n_2 = 0$ in (n_1, n_2) and the SWCNT is called *zigzag*. On the other hand, the SWCNT is called *armchair* when $\theta = \pi/6$ and n_1 is equal to n_2. For any other value in the range $(0; \pi/6]$, the nanotube is referred to as *chiral*.

Moreover, the chiral vector $\mathbf{C}_h$ can be used to identify the periodic unit cells of the carbon nanotubes. Indeed, as

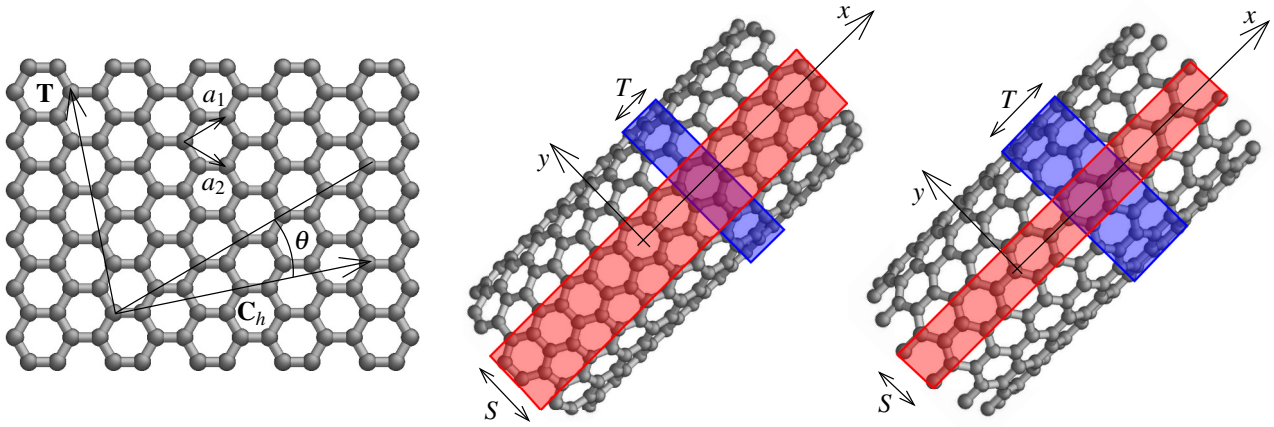

(a) graphene sheet (b) (8,8) armchair (c) (14,0) zigzag

Figure 2: (a) Honeycomb structure of graphene and atomic configuration of (b) an $(8,8)$ armchair and (c) a $(14,0)$ zigzag SWCNT. Blue and red areas denote the portions of SWCNT which are repeated periodically along the longitudinal axis and the circumference, respectively.

indicated in Figure 2(b)–(c), an SWCNT is periodic along both the longitudinal and the circumferential directions. In particular, the width of the periodic unit cell along the nanotube axis is

$$T = |\mathbf{T}| = \frac{\sqrt{3}\,|\mathbf{C}_h|}{\gcd(2n_1+n_2, 2n_2+n_1)}, \tag{11}$$

where $|\mathbf{T}|$ denotes the magnitude of the translational vector $\mathbf{T}$ (see Figure 2(a)) and $\gcd(a,b)$ the greatest common divisor (gcd) of two integers a and b. Similarly, the width of the periodic cell along the circumference is

$$S = \frac{|\mathbf{C}_h|}{\gcd(n_1,n_2)}. \tag{12}$$

As shown in Figure 2, the widths T and S vary according to the chirality of the nanotube while they are not affected by its diameter and length.

For more details on the periodicity and symmetry of SWCNT structure we refer the reader to Ref. [32].

2.3. Young's modulus

By assuming the carbon nanotubes as continuum hollow cylinders, a set of SWCNTs with different diameter and chirality has been employed to derive the Young's modulus E_{xx} for the one-dimensional formulation in Section 3. One end of the nanotube was fully constrained whereas an axial displacement $\bar{u}_x$ was applied to the opposite side where radial displacements are also constrained. The value of $\bar{u}_x$ was set equal to 10^{-5} nm in order to calculate the tangent elastic modulus of the nanotubes and to satisfy the small deformation hypothesis. We stress that the nonlinear

constitutive laws of the structural elements in the MSM model, which are representative of the covalent bonds, do not account for plasticity and damage.

Figure 4 shows the deformed configurations of a tensile SWCNT. The value of the stiffness was determined through

$$E_{xx} = F_x L / A \bar{u}_x, \tag{13}$$

where F_x is the reaction force along the longitudinal direction at the fully constrained end, and A is the cross sectional area of the SWCNT. This quantity is defined as the area of an annulus with thickness $t = 0.34$ nm [33] and inner diameter $d - t/2$. The results, shown in Figure 3 and in Tables 1 and 2, reveal a dependence on diameter and chirality. Indeed, E_{xx} increases with the diameter and reaches an almost constant value for d larger than 2 nm. The two sets of chiral SWCNTs yield the highest values of E_{xx}, whereas zigzag nanotubes have the lowest axial stiffness.

These results are in good agreement with experimental and numerical tests in the literature. Demczyk et al. [34] estimated a Young's modulus equal to 900 GPa from pulling individual carbon nanotubes with diameter of about 10 nm away from one fixed end in a transition electron microscope. Values of E_{xx} ranging between 940 and 1118 GPa have been found with *ab initio* calculations in Ref. [35]. Based on molecular dynamics simulations, WenXing et al. [36] showed that the Young's modulus ranges between 918 and 941 GPa for SWCNTs with different chirality and diameters ranging between 1.6 and 2.8 nm. Belytschko et al. [4] calculated a value of E_{xx} equal to 940 GPa for a $(20,0)$ nanotube with the modified Morse potential in molecular mechanics calculations. Meo and Rossi [37], by employing an MSM approach similar to that presented in this paper to SWCNTs with diameter ranging between 0.4 and 2 nm, showed that the Young's modulus varies from 910 to 923 GPa for the armchair configuration and from 899 and 920 GPa for the zigzag configuration. Furthermore, similar effects of chirality on the elastic modulus have been observed in Refs. [6, 38–40].

(n_1,n_1)	d [nm]	E_{xx} [GPa]
$(4,4)$	0.54	905.4
$(8,8)$	1.09	919.9
$(12,12)$	1.63	923.1
$(16,16)$	2.17	924.4
$(20,20)$	2.71	925.2
$(24,24)$	3.26	925.7
$(28,28)$	3.80	926.1
$(32,32)$	4.34	926.4
$(40,40)$	5.43	926.9

(a) (n_1,n_1) armchair

$(n_1,0)$	d [nm]	E_{xx} [GPa]
$(6,0)$	0.47	871.6
$(14,0)$	1.10	908.7
$(20,0)$	1.57	913.8
$(26,0)$	2.04	915.1
$(32,0)$	2.51	917.1
$(38,0)$	2.98	917.9
$(44,0)$	3.45	918.4
$(56,0)$	4.39	919.0
$(64,0)$	5.01	919.4

(b) $(n_1,0)$ zigzag

Table 1: Young's modulus of (a) armchair and (b) zigzag SWCNTs with a length of 12.31 and 12.36 nm, respectively.

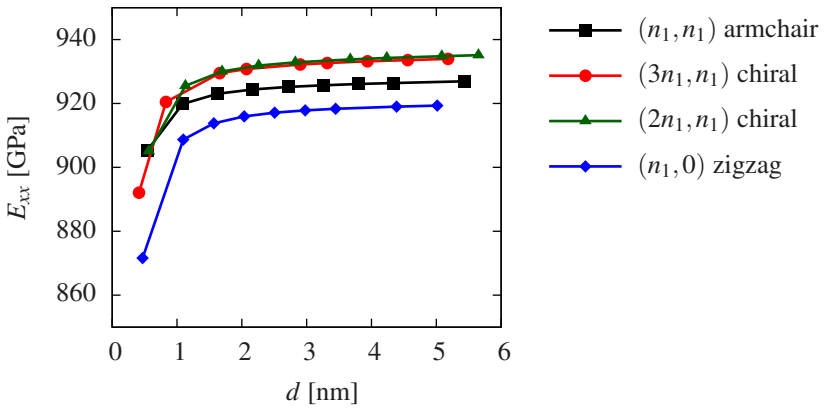

Figure 3: Young's modulus of SWCNTs as a function of diameter and chirality.

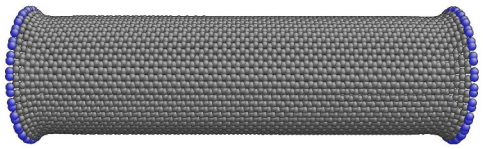

Figure 4: Deformed configuration of a $(28,28)$ armchair SWCNT with length 12.31 nm under tensile loading (blue atoms have constrained radial displacements).

$(2n_1,n_1)$	d [nm]	E_{xx} [GPa]
$(4,2)$	0.41	892.1
$(8,4)$	0.83	920.5
$(16,8)$	1.66	929.5
$(20,10)$	2.07	930.8
$(28,14)$	2.90	932.2
$(32,16)$	3.32	932.7
$(38,19)$	3.94	933.2
$(44,22)$	4.56	933.6
$(50,25)$	5.18	933.7

(a) $(2n_1,n_1)$ chiral

$(3n_1,n_1)$	d [nm]	E_{xx} [GPa]
$(6,2)$	0.56	905.1
$(12,4)$	1.13	925.5
$(18,6)$	1.69	930.0
$(24,8)$	2.26	931.9
$(30,10)$	2.82	932.9
$(39,13)$	3.67	933.8
$(45,15)$	4.24	934.3
$(54,18)$	5.08	934.8
$(60,20)$	5.65	935.1

(b) $(3n_1,n_1)$ chiral

Table 2: Young's modulus for (a) $(2n_1,n_1)$ and (b) $(3n_1,n_1)$ chiral SWCNTs with a length of 12.41 and 12.30 nm, respectively.

2.4. Strain field in SWCNTs under tensile load

To investigate the axial strain in tensile SWCNTs, we adopt the technique developed by Shimizu et al. [41] who calculate the strain field from atomistic simulations. The idea behind this method is that strains are calculated through a least-squares fit of the deformation gradient $\mathbf{J}_i$ for each atom i. Accordingly, $\mathbf{J}_i$ is computed as the tensor which best

maps

$$\{\mathbf{d}_{ij}\} \longrightarrow \{\mathbf{d}^0_{ij}\} \tag{14}$$

where $\mathbf{d}_{ij}$ and $\mathbf{d}^0_{ij}$ are the distances between atom i and its neighbor j in the current and reference configuration, respectively. Therefore, minimization of

$$\sum_{i\in N_i} \left|\mathbf{J}_i\mathbf{d}^0_{ij} - \mathbf{d}_{ij}\right|^2,$$

yields the deformation gradient

$$\mathbf{J}_i = \left(\sum_{i\in N_i} \mathbf{d}^{0T}_{ij}\mathbf{d}^0_{ij}\right)^{-1}\left(\sum_{i\in N_i} \mathbf{d}^{0T}_{ij}\mathbf{d}_{ij}\right), \tag{15}$$

in which N_i denotes the number of neighbors of atom i. The value of N_i depends on the cutoff radius r_{co} since it specifies the region of the nanotube to be considered in the calculation. Here, we assume r_{co} equal to the magnitude of the Burgers vector in carbon nanotubes [42], namely $\sqrt{3}a_{cc}$. Therefore, with $\mathbf{I}$ denoting the identity tensor, the Lagrangian strain tensor at atom i is defined as [41]

$$\mathbf{E}_i = \frac{1}{2}\left(\mathbf{J}_i\mathbf{J}_i^T - \mathbf{I}\right). \tag{16}$$

Next, we will examine the influence of chirality on the axial component ε_{xx} of the strain field derived from (16) and the circumferential strain field ε_r calculated as the ratio between the radial displacement u_r and the nanotube radius. Here and throughout the paper, ε_{xx} and ε_r are normalized with respect to local axial strain $\bar{\varepsilon}_{xx} = \bar{u}_x/L$ and the circumferential strain at the middle section $\varepsilon_{r,x/L=0.5}$, respectively.

To investigate the effect of the chirality, strain field is represented on the unrolled nanotube. The normalized strain field values at atoms aligned along the longitudinal direction are interpolated by piecewise curves as depicted in Figure 5 where ε_{xx} and ε_r are shown for three tensile nanotubes with different chirality but similar diameter and length. Furthermore, All nanotubes show a boundary layer. In armchair and zigzag nanotubes, both axial and circumferential strain fields are represented by two different curves with similar trend which repeat periodically along the circumference. Chiral nanotubes, on the other hand, present a higher number of periodic curves and a more complex profile of the strain field due to the rotation of the symmetry axis. Chirality-induced anisotropy in chiral SWCNTs has been discussed in many works [43–45]. However, only few studies aimed at modeling chiral nanotubes as anisotropic

shells [10, 46, 47] instead of using the more common isotropic models [7, 48–53]. Unfortunately, none of these works has included a comparison of the strain field obtained with atomistic simulations and shell models. Moreover, it is likely that continuum models cannot reproduce the complex profile of the strain field reported in Figures 5(e) and 5(f) which is a consequence of the discrete structure of the nanotube.

With regard to the diameter, we compare the strain field in nanotubes with equal chirality and length but different diameter. Figure 6(a)-(b) shows that height and width of the boundary layer increase with the diameter d in both armchair and zigzag SWCNTs. A similar dependence of ε_{xx} on the diameter, as shown in Figure 6(c)-(d), is observed in chiral nanotubes. With regard to the radial strain, Figure 7 shows that the width of the boundary layer increases with the nanotube diameter, whereas its height barely changes.

Finally, the dependence of the strain profile on the nanotube length has been examined. We observed that the effect of L on both ε_{xx} and ε_r is negligible (refer to the discussion in Section 4).

The MSM results presented in this Section have been verified with those obtained from MM simulations performed with the LAMMPS software [54] (codes are freely available for download at the authors web page).

3. Nonlocal integro-differential elastic model for one-dimensional problems

According to the nonlocal theory of elasticity developed by Eringen [15], the strain at a point is calculated as a weighted integral of the strain field at surrounding points. By accounting for small-scale effects, nonlocal theories have been used to model nonastructures such as carbon nanotubes [17, 18]. Hence, with the aim of modeling tensile SWCNTs as one-dimensional rods with mechanical properties that can be related to those of SWCNTs, the local/nonlocal constitutive law

$$\sigma_{xx}(x) = E_{xx}\left(\xi_1 \varepsilon_{xx}(x) + \xi_2 \int_0^L g\left(x,\bar{x},\ell\right) \varepsilon_{xx}(\bar{x})\, \mathrm{d}\bar{x}\right) \tag{17}$$

proposed in Ref. [23] is adopted in this work. Parameters ξ_1 and ξ_2 are such that $\xi_1 + \xi_2 = 1$ (see [24]), and the nonlocal kernel $g\left(x,\bar{x},\ell\right)$ is a weighting function which depends on the distance $|x-\bar{x}|$ and the intrinsic length scale ℓ of the nanotubes (which is related to its geometry).

The choice of a nonlocal kernel capable of representing long-range atomic interactions is crucial for the accurate prediction of deformation phenomena at the nanoscale. In the literature, Gaussian and exponential weight functions have been widely used [23]. With these kernels, however, the nonlocal model used in this study was not able to accurately reproduce the axial strain field obtained with MSM. Fortunately, this was possible with the atomistically-

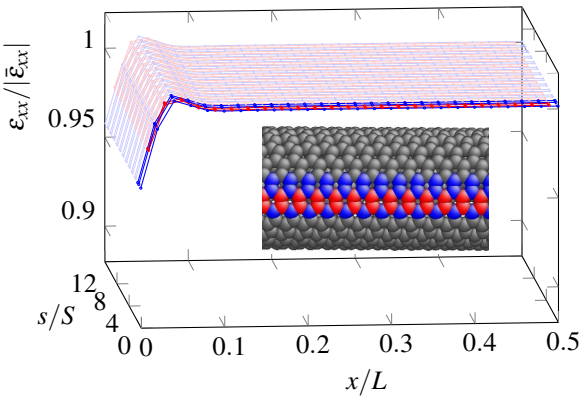

(a) (12,12) armchair

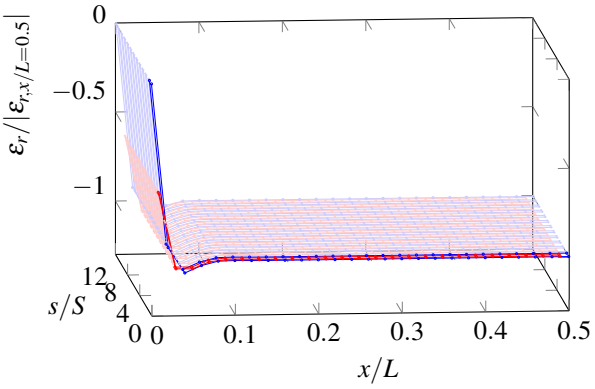

(b) (12,12) armchair

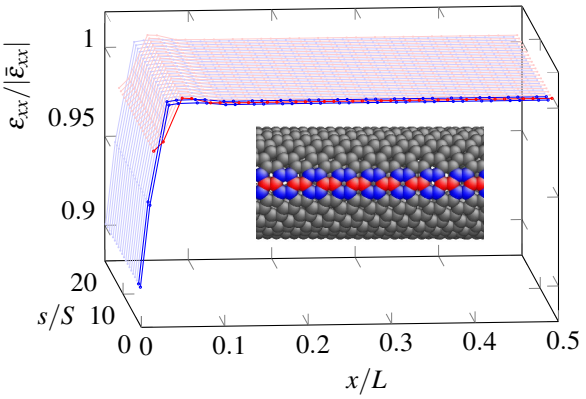

(c) (20,0) zigzag

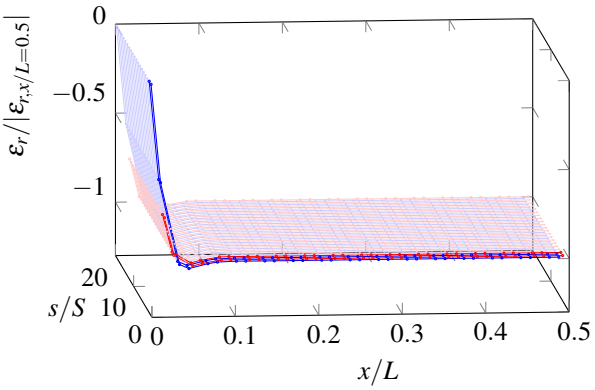

(d) (20,0) zigzag

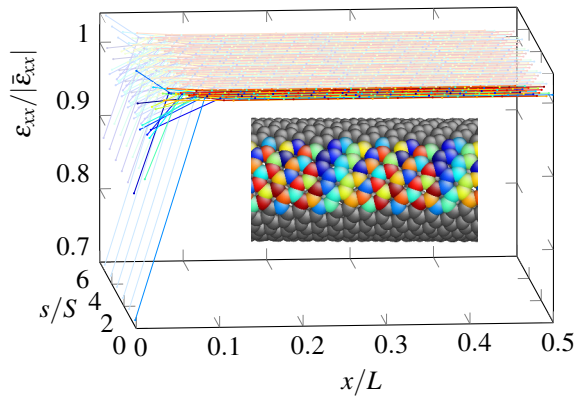

(e) (18,6) chiral

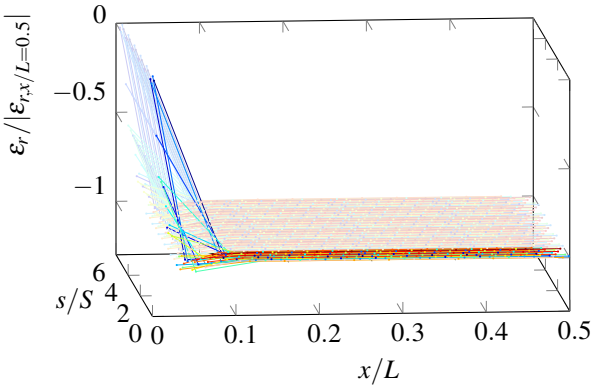

(f) (18,6) chiral

Figure 5: Normalized axial and hoop strain fields in (a)-(b) $(12,12)$ armchair, (c)-(d) $(20,0)$ zigzag and (e)-(f) $(18,6)$ chiral SWCNTs. The strain field is represented over the unrolled SWCNTs surface. Only half of the axial domain is shown due to symmetry, whereas the entire curvilinear abscissa s, related to the circumference of the nanotubes, is considered. The atoms aligned along the x direction are connected with a piecewise linear interpolation. Lines whose atoms are aligned along the s direction have the same color. For illustration purposes, only the lines in the first periodic longitudinal strip of width S have been highlighted (make reference to Figure 2 for the definition of S). The insets provide a visual representation of the SWNTCs atomic structure and of the highlighted lines of atoms: five in the armchair configuration, three in the zigzag configuration and 26 in the chiral configuration.

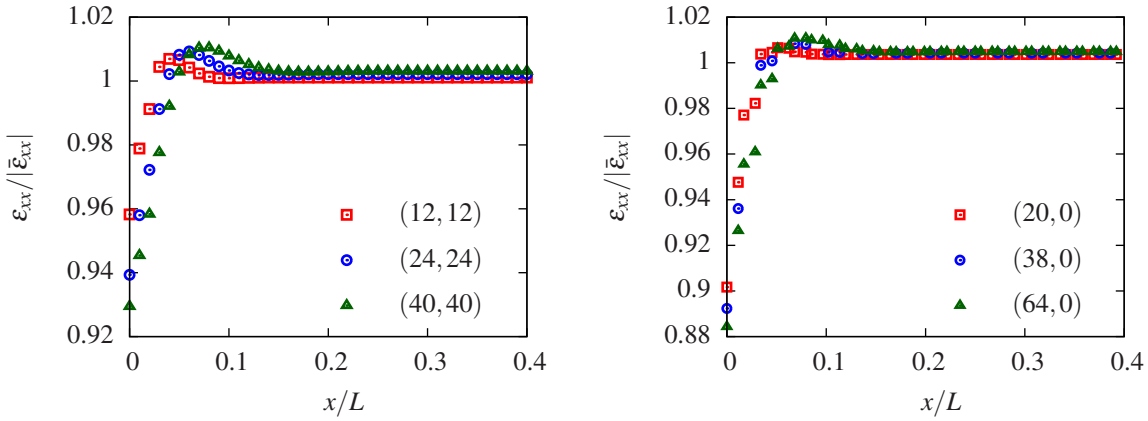

(a) (n_1,n_1) armchair

(b) $(n_1,0)$ zigzag

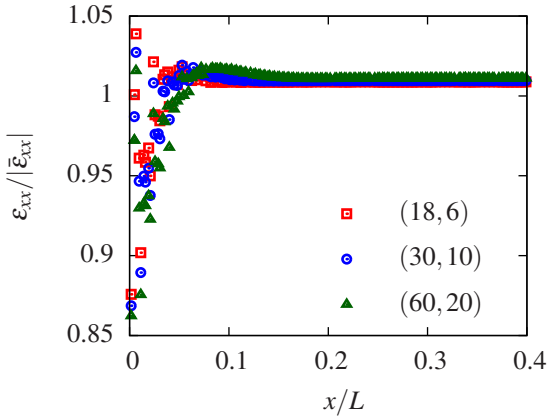

(c) $(3n_1,n_1)$ chiral

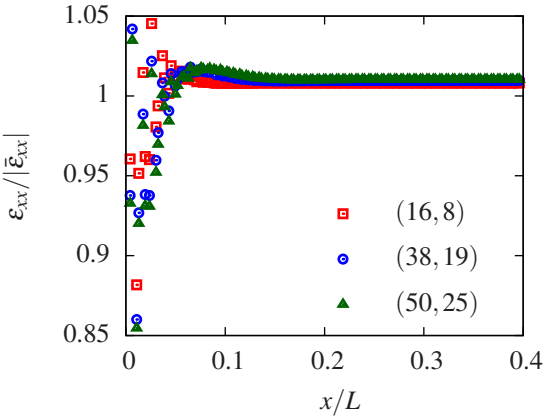

(d) $(2n_1,n_1)$ chiral

Figure 6: Normalized axial strain field for (a) armchair, (b) zigzag, (c) $(3n_1,n_1)$ chiral and (c) $(2n_1,n_1)$ chiral SWCNTs.

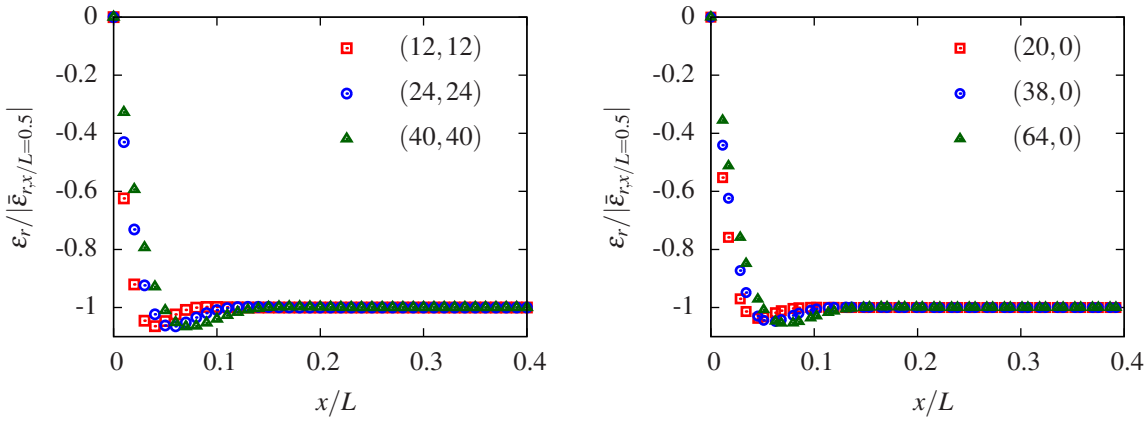

(a) (n_1,n_1) armchair

(b) $(n_1,0)$ zigzag

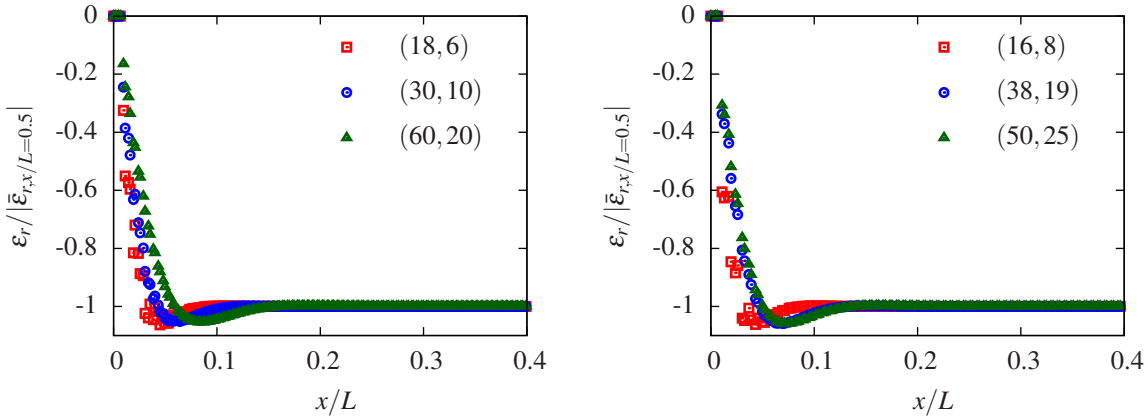

(c) $(3n_1,n_1)$ chiral

(d) $(2n_1,n_1)$ chiral

Figure 7: Normalized hoop strain field for (a) armchair, (b) zigzag, (c) $(3n_1,n_1)$ chiral and (c) $(2n_1,n_1)$ chiral SWCNTs.

based nonlocal kernel

$$g\left(x,\bar{x},mb\right) = \alpha_0 \left(1 - n\left(\left|x-\bar{x}\right|/b\right)^2\right) \exp\left[-\left(\left|x-\bar{x}\right|/mb\right)^2\right] \tag{18}$$

proposed by Picu [25], where the intrinsic length scale ℓ is defined as the product of the nonlocal parameter m and the magnitude b of the Burgers vector $\mathbf{b}$. A second dimensionless nonlocal parameter, n, and the normalization factor α_0 complete the set of parameters. In the one-dimensional case, the condition

$$\int_0^L g\left(x,\bar{x},\ell\right) \mathrm{d}\bar{x} = 1. \tag{19}$$

yields

$$\alpha_0 = \left[\sqrt{\pi} mb \left(1 - 0.5nm^2\right)\right]^{-1}. \tag{20}$$

3.1. Numerical solution

To understand the physical implications of the nonlocal parameters in (18), we make use of a representative one-dimensional problem. We consider an elastic rod with length L, cross sectional area A and Young's modulus E_{xx} equal to 20 nm, 1 nm^2 and 900 GPa, respectively. An axial displacement $\bar{u} = 1$ nm is applied at $x = L$ while the opposite end at $x = 0$ mm is fixed. This boundary value problem has been solved numerically since the analytical solution is not available. As shown in Ref. [55], higher order B-spline basis functions are superior to classical Lagrange and Hermite basis functions and C^∞ generalized finite element approximations in modeling nonlocal integro-differential problems. In general, B-spline basis functions avoid the presence of periodic oscillations which, on the contrary, characterize the strain field approximated with the other techniques. Therefore, in this work, quintic B-spline basis functions have been employed for the computation of ε_{xx}. The one-dimensional model has been discretized using 107 equally-spaced elements (usually referred to as uniform knot spans in the isogeometric analysis context [56]) which correspond to 100 degrees of freedom. The MATLAB® scripts are freely available for download[1] as supplementary material of Ref. [55].

As indicated in Figure 8(a), the discrepancy between nonlocal and local solution (which corresponds to $\xi_1 = 1$) increases with $|1-\xi_1|$. For $\xi_1 > 1$ the value of ε_{xx} at the boundaries is smaller than the local strain $\bar{\varepsilon}_{xx}$, whereas $\xi_1 < 1$ produces the opposite behavior. Figure 8(b) shows that the boundary layer becomes sharper by decreasing m as a consequence of the smaller intrinsic length scale ℓ. These results are similar to those derived by Benvenuti and

[1] http://sourceforge.net/projects/nonlocal-gradient-elasticity1d/

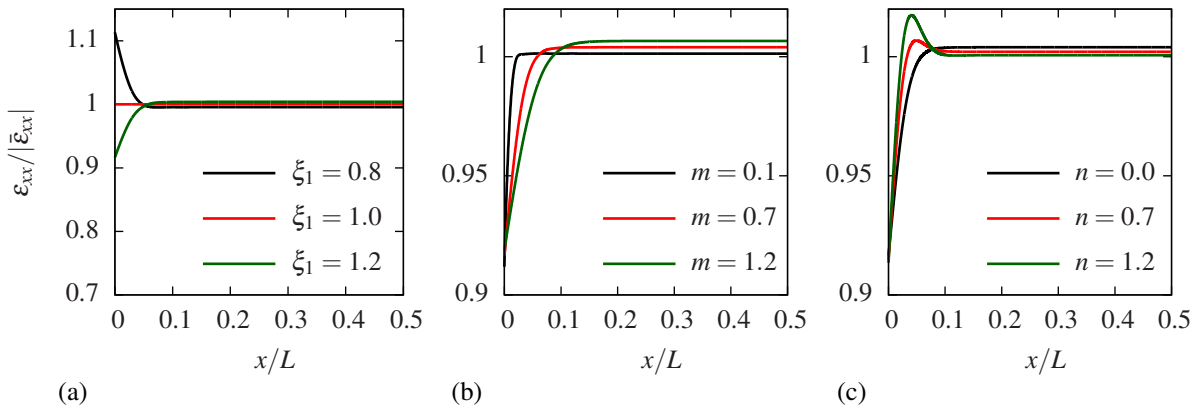

Figure 8: Normalized strain field for a one-dimensional nonlocal tensile rod by fixing (a) $m = 0.7$ and $n = 0$, (b) $\xi_1 = 1.2$ and $n = 0$, (c) $\xi_1 = 1.2$ and $m = 0.7$, and by varying ξ_1, m and n, respectively.

Simone [24] with of an exponential kernel. Nonetheless, the presence of the second nonlocal parameter n leads to an interesting consequence. Indeed, as illustrated in Figure 8(c), n increases the maximum value of the strain toward the boundary layers. Consequently, the profile of ε_{xx} obtained from the one-dimensional nonlocal model recalls the results calculated with molecular structural mechanics.

Hence, it might be interesting to provide a reliable estimate of the nonlocal parameters ξ_1, m and n in oder to approximate the axial strain field of tensile SWCNTs with the nonlocal model (17) equipped with the atomistically-based kernel (18). To achieve this goal, we will make use of a parameter estimation procedure. This procedure is feasible for the axial strain field in armchair and zigzag nanotubes due to the similarity of the strain profiles in the periodic strip. As shown in Figure 6(c)-(d), a similar argument does not hold for the response of chiral SWCNTs. Therefore, in the parameter estimation procedure described in the next section we will derive ξ_1, m and n only for armchair and zigzag nanotubes.

4. Estimation of the nonlocal parameters

Based on the collection of results provided by the atomistic simulations described in Section 2, we wish to determine the value of the parameters m, n and ξ_1 for each SWCNT such that the nonlocal model can accurately represents the axial strain field calculated with MSM. This operation is performed by means of a parameter estimation procedure. Given the parameter vector $p = [\xi_1, m, n]$, we aim to solve the least-square problem

$$\min_p f(p), \tag{21}$$

where the objective function

$$f(p) = \frac{1}{2}\sum_{i=1}^{N}\left(\frac{\varepsilon_{xx_i}^{NL}(p) - \varepsilon_{xx_i}^{MSM}}{\bar{\varepsilon}}\right)^2 \tag{22}$$

measures the discrepancy between nonlocal and MSM results at the N points corresponding to the atoms of the SWCNT. To improve the quality of the fit for the boundary layers in ε_{xx}, we consider problem (21) subject to the inequality constraints

$$c(p) = \frac{\left|\varepsilon^{NL}(x_m,p) - \varepsilon^{MSM}(x_m)\right|}{\varepsilon^{MSM}(x_m)} \leq \tau \qquad \text{and} \qquad C(p) = \frac{\left|\varepsilon^{NL}(x_M,p) - \varepsilon^{MSM}(x_M)\right|}{\varepsilon^{MSM}(x_M)} \leq \tau \tag{23}$$

where x_m and x_M denote the minimum and maximum values of the atomic strain field, and the tolerance τ is assumed equal to 10^{-6}.

Constrained parameter estimation problems can be solved with different numerical techniques [27]. For our purposes, we used the quadratic penalty method. This simple technique combines objective function (22) and constraints (23) into the unconstrained optimization problem

$$\min_p \left\{ Q(p,\mu) = f(p) + \frac{\mu}{2}\sum\left(c^2(p) + C^2(p)\right)\right\}, \tag{24}$$

in which the penalty parameter μ penalizes constraint violations —that is, the higher the value of μ the closer to zero the constraints in (23). The quadratic penalty method may lead to ill conditioning and unfeasible solutions. Nonetheless, as suggested in Ref. [27], it is possible to avoid these issues by choosing a suitable sequence of positive values $\{\mu_k\}$ with $\mu_k \to \infty$ as $k \to \infty$ and to calculate the approximate minimizer p_k of $Q(p,\mu_k)$ for each k.

Hence, for each nanotube a reasonable starting point p_0 of the identification process was carried out with a preliminary visual examination and the initial penalty parameter μ_0 was assumed equal to 1. The set of parameters $\{\mu_k\}$ has been chosen such that $\mu_k = 10\mu_{k-1}$. At each k-th step an approximate minimizer p_k of $Q(p,\mu_k)$ was derived by starting from $p = p_{k-1}$ and terminating either when the objective function $Q(p,\mu_k)$ was less than 10^{-4} or the infinity norm of the gradient $\nabla_p Q(p,\mu_k)$ was less than 10^{-6}. By satisfying these requirements, the minimizer of $Q(p,\mu_k)$ was reached. In particular, the Gauss-Newton method was used to minimize the objective function in (24) avoiding the trouble of computing the Hessian of $Q(p,\mu_k)$ [27]. In general, it was observed that a small number of iterations was needed to attain the converged solution as reported in Figure 9. This iterative procedure was repeated until the feasibility conditions (23) were satisfied.

To investigate the influence of the nanotube length on the nonlocal parameters, we have considered several values

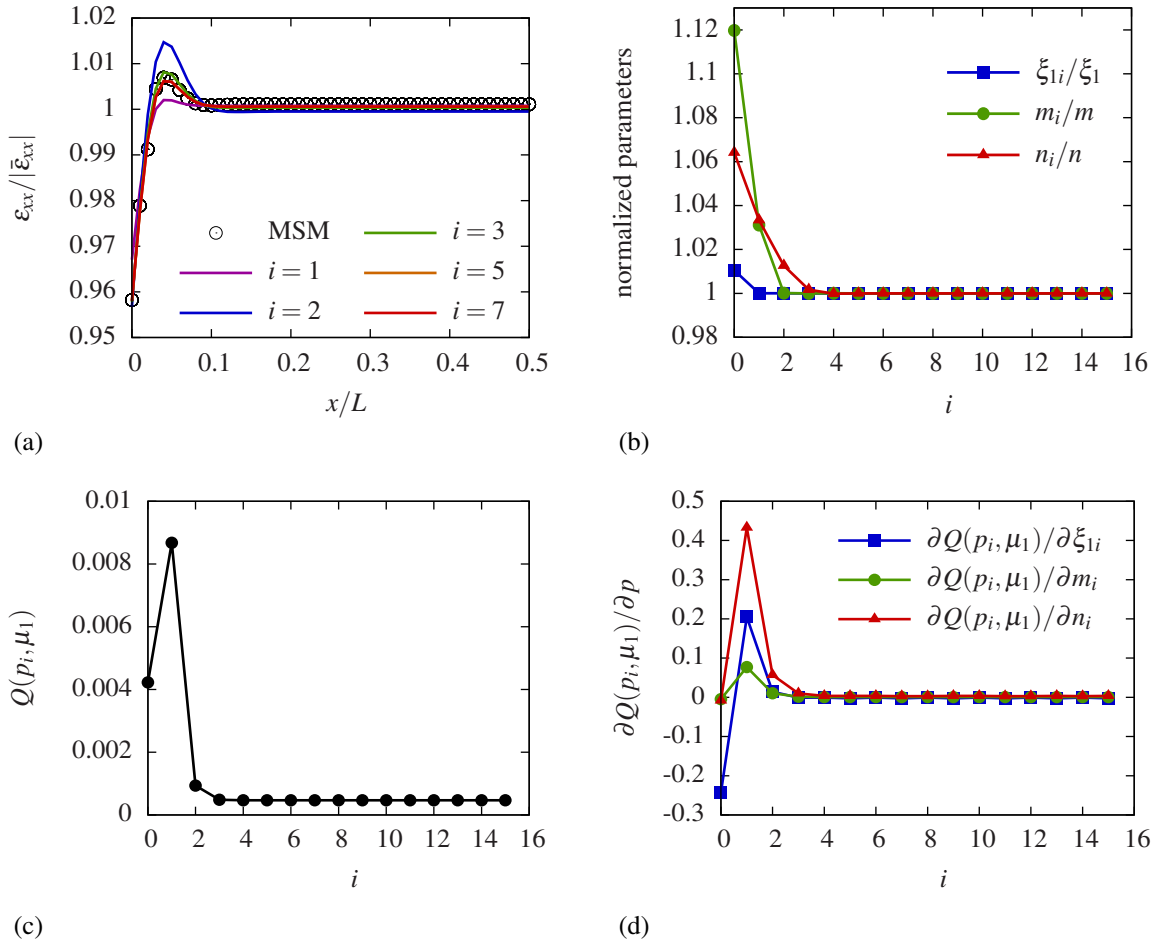

Figure 9: Convergence pattern of the initial k-th step (i.e. $\mu_k = \mu_1$) for the $(12,12)$ armchair SWCNT: (a) normalized nonlocal axial strain field approximating the MSM results (only few iteration steps are displayed), (b) normalized values of the nonlocal parameters ξ_1, m and n, (c) the cost function and (d) its derivatives with respect to p (i refers to the iteration number).

of L. First, ξ_1, m and n have been estimated for armchair and zigzag nanotubes with a length of 12.31 and 12.36 nm, respectively. Quintic B-spline basis functions, 400 degrees of freedom and uniform knot spans have been used while computing ε_{xx}^{NL}. Then, we have considered SWNCTs whose length was two, four and eight times longer then the previous ones. Accordingly, the nonlocal strain field has been calculated by increasing the number of degrees of freedom involved in the analysis two, four and eight times (i.e. by keeping the size of the knots spans constant).

Figure 10 illustrates the calculated nonlocal parameters corresponding to armchair and zigzag nanotubes with different diameters and lengths. As mentioned in Section 2.4, the diameter has a marked effect in the characterization of the strain field of SWCNTs whereas length effects are negligible. Furthermore, we can easily notice a clear trend in the value of ξ_1, m and n. Therefore, seeking for an analytical relation between the nonlocal parameters and the nanotubes geometric characteristics we have considered the function

$$q(d,\theta) = c_1(\theta) + c_2(\theta)\, d^{\,c_3(\theta)} \tag{25}$$

where q is a generic nonlocal parameter, equal to m, n or ξ_1. The dimensionless parameters c_1, c_2 and c_3 have been determined for both armchair and zigzag nanotubes with the *fit* function from the MATLAB® Optimization Toolbox. In particular, the Trust-Region algorithm with randomly generated starting points has been chosen. The estimated set of parameters is listed in Table 3 and the corresponding functions are depicted in Figure 10.

	ξ_1	m	n
c_1	1.48	−2.96	0.05
c_2	−0.16	4.43	0.43
c_3	−0.22	0.22	−1.83
RMSE	3.99e−7	5.07e−6	8.83e−5
R^2	0.9995	0.9989	0.9980

(a) (n_1,n_1) armchair

	ξ_1	m	n
c_1	1.12	0.26	0.70
c_2	0.11	1.17	−0.49
c_3	0.31	0.42	0.14
RMSE	3.38e−6	1.44e−4	4.74e−5
R^2	0.9864	0.9490	0.9922

(b) $(n_1,0)$ zigzag

Table 3: Parameter c_1, c_2 and c_3 for (a) armchair and (b) zigzag nanotubes with diameter ranging between 1 and 5.5 nm. The goodness of fit has been assessed by calculating the root mean square error (RMSE) and the coefficient of determination (R^2).

To conclude, we have assessed the effectiveness of the proposed model. As illustrated in Figure 11, the one-dimensional nonlocal model (17), with ξ_1, m and n derived from (25), yields a good approximation of the axial strain field in tensile SWCNTs. However, despite an accurate approximation of the boundary layers, a small discrepancy between discrete and continuum profiles occurs in the central part of the domain as shown in the insets in Figure 11. Nonetheless, it was observed that such discrepancy decreases by increasing the length of the nanotubes. Furthermore, we have compared the total strain energy computed with MSM (Π^{MSM}) and the nonlocal theory (Π^{NL}). As reported in Figure 12, the relative error is small. This discrepancy does not lie only in the approximation provided by the nonlocal

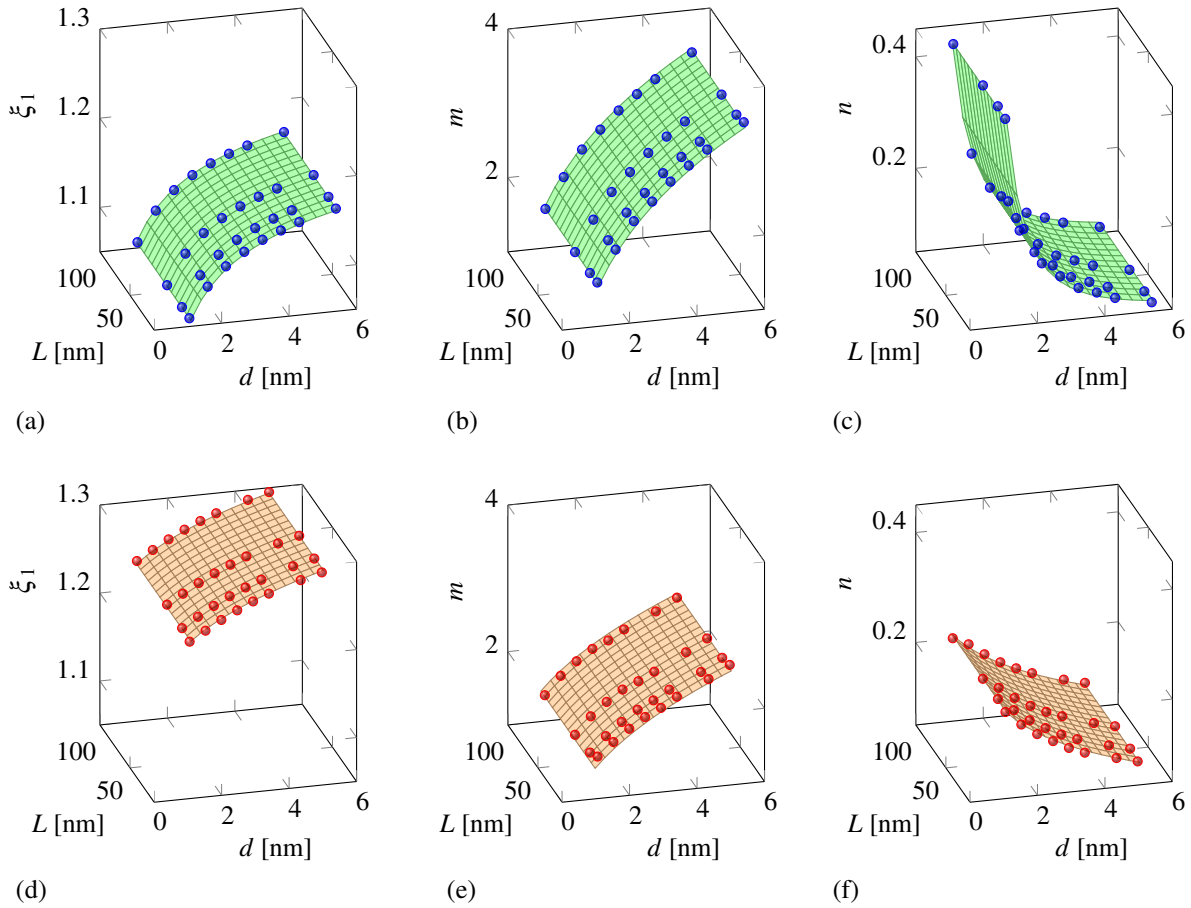

Figure 10: Nonlocal parameters ξ_1, m and n for (a)-(c) (n_1,n_1) armchair and (d)-(f) $(n_1,0)$ zigzag SWCNTs calculated with the parameter estimation procedure (filled markers) and corresponding approximating surface.

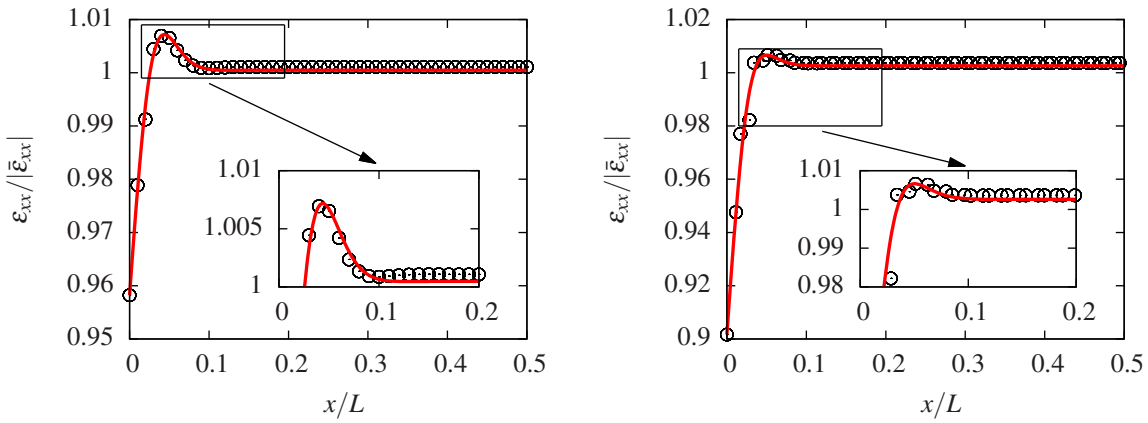

(a) (12,12) armchair (b) (20,0) zigzag

Figure 11: Normalized axial strain field ε_{xx} calculated with MSM simulations (circles) and the one-dimensional nonlocal model (solid red line) for (a) a $(12,12)$ armchair and (b) a $(20,0)$ zigzag SWCNTs with length L equal to 12.31 and 12.05 nm, respectively.

formulation. Indeed, it can also be attributed to the deformation components involved in the calculation of the strain energy. For the nonlocal one-dimensional model, Π^{NL} is determined solely by the axial deformations. In contrast, for the atomistic simulation, Π^{MSM} is expressed as a summation of different terms (see eq. (1)) from which it is not possible to derive the components specifically related to axial deformations.

5. Conclusions

We have estimated the parameters required to model tensile SWCNTs as nonlocal rods. With these parameters it was possible to correctly capture size and chirality effects observed in the axial strain profile computed with molecular structural mechanics. In particular, the optimal nonlocal parameters resulted to vary with the diameter and the chirality of the nanotubes while the influence of the length was negligible. Nonlocal parameters have been estimated for armchair and zigzag SWCNTs only. As the orthotropy axes in chiral SWCNTs are not aligned with the chiral and roll-up axes, one-dimensional theories are not suitable.

The choice of the nonlocal kernel was the key to the characterization of the equivalent nonlocal rod model. By adopting an atomistically-based nonlocal kernel, the axial strain profiles obtained with the integro-differential formulation were remarkably consistent with those predicted with molecular structural mechanics. Classical Gaussian and exponential kernels did not produce similar results.

The successful use of nonlocal models as a replacement for more sophisticated atomistic models hinges on the reliable determination of the nonlocal parameters and the choice of the constitutive relation. To our knowledge, this is the first time nonlocal parameters have been derived from the axial strain field obtained from atomistic simulations of

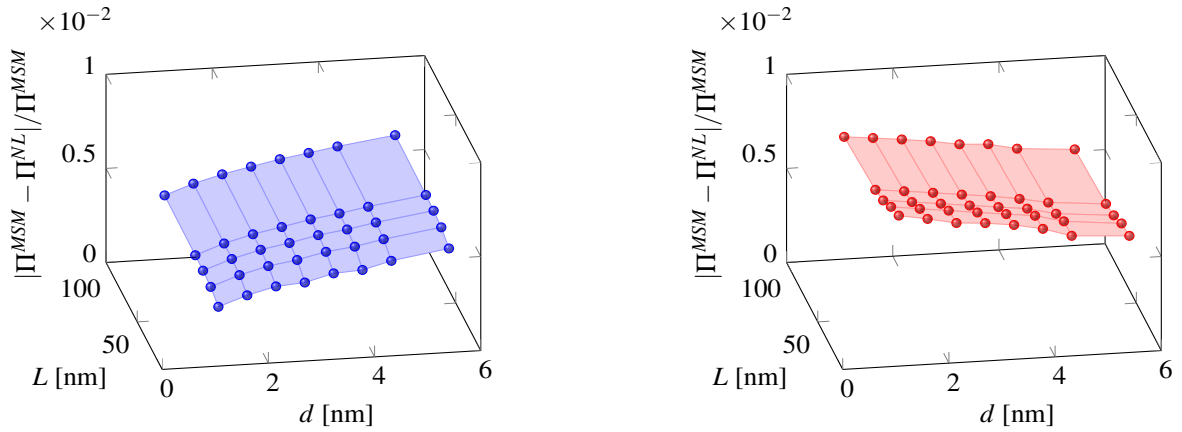

(a) (n_1, n_1) armchair (b) $(n_1, 0)$ zigzag

Figure 12: Relative error between the total strain energies computed with MSM (Π^{MSM}) and the one-dimensional nonlocal model (Π^{NL}) for (a) armchair and (b) zigzag SWCNTs.

SWCNTs. The adopted approach, although partially successful because applicable to "smooth" axial strain profiles only, paves the way for the use of nonlocal formulations in studies of CNTs and CNTs-based composites and all those applications in which axial deformation is the predominant CNT deformation mode.

References

[1] R. Rafiee, R. M. Moghadam, On the modeling of carbon nanotubes: A critical review, Composites part B: Engineering 56 (2014) 435–449.

[2] D. Sánchez-Portal, E. Artacho, J. M. Soler, A. Rubio, P. Ordejón, Ab initio structural, elastic, and vibrational properties of carbon nanotubes, Physical Review B 59 (1999) 12678.

[3] K. M. Liew, X. Q. He, C. H. Wong, On the study of elastic and plastic properties of multi-walled carbon nanotubes under axial tension using molecular dynamics simulation, Acta Materialia 52 (2004) 2521–2527.

[4] T. Belytschko, S. P. Xiao, G. C. Schatz, R. S. Ruoff, Atomistic simulations of nanotube fracture, Physical Review B 65 (2002) 235430.

[5] C. Li, T.-W. Chou, A structural mechanics approach for the analysis of carbon nanotubes, International Journal of Solids and Structures 40 (2003) 2487–2499.

[6] K. I. Tserpes, P. Papanikos, Finite element modeling of single-walled carbon nanotubes, Composites part B: Engineering 36 (2005) 468–477.

[7] B. I. Yakobson, C. J. Brabec, J. Bernholc, Nanomechanics of carbon tubes: instabilities beyond linear response, Physical Review B 76 (1996) 2511.

[8] J. P. Lu, Elastic properties of carbon nanotubes and nanoropes, Physical Review Letters 79 (1997) 1297.

[9] Z. Xin, Z. Jianjun, O. Zhong-Can, Strain energy and youngs modulus of single-wall carbon nanotubes calculated from electronic energy-band theory, Physical Review B 62 (2000) 13692.

[10] T. Chang, A molecular based anisotropic shell model for single-walled carbon nanotubes, Journal of the Mechanics and Physics of Solids 58 (2010) 1422–1433.

[11] P. Poncharal, Z. Wang, D. Ugarte, W. A. De Heer, Electrostatic deflections and electromechanical resonances of carbon nanotubes, Science 283 (1999) 1513–1516.

[12] J. Yoon, C. Q. Ru, A. Mioduchowski, Timoshenko-beam effects on transverse wave propagation in carbon nanotubes, Composites Part B: Engineering 35 (2004) 87–93.

[13] N. Yao, V. Lordi, Youngs modulus of single-walled carbon nanotubes, Journal of Applied Physics 84 (1998) 1939–1943.

[14] T. Chang, J. Geng, X. Guo, Prediction of chirality-and size-dependent elastic properties of single-walled carbon nanotubes via a molecular mechanics model, Proceedings of the Royal Society A: Mathematical, Physical and Engineering Science 462 (2006) 2523–2540.

[15] A. C. Eringen, On differential equations of nonlocal elasticity and solutions of screw dislocation and surface waves, Journal of Applied Physics 54 (1983) 4703–4710.

[16] L. J. Sudak, Column buckling of multiwalled carbon nanotubes using nonlocal continuum mechanics, Journal of Applied Physics 94 (2003) 7281–7287.

[17] Y. Q. Zhang, G. R. Liu, X. Y. Xie, Free transverse vibrations of double-walled carbon nanotubes using a theory of nonlocal elasticity, Physical Review B 71 (2005) 195404.

[18] B. Arash, Q. Wang, A review on the application of nonlocal elastic models in modeling of carbon nanotubes and graphenes, Computational Materials Science 65 (2012) 303–313.

[19] W. H. Duan, C. M. Wang, Y. Y. Zhang, Calibration of nonlocal scaling effect parameter for free vibration of carbon nanotubes by molecular dynamics, Journal of Applied Physics 101 (2007) 024305–024305.

[20] Y. G. Hu, K. M. Liew, Q. Wang, Nonlocal continuum model and molecular dynamics for free vibration of single-walled carbon nanotubes, Journal of nanoscience and nanotechnology 11 (2011) 10401–10407.

[21] F. Khademolhosseini, A. S. Phani, A. Nojeh, N. Rajapakse, Nonlocal continuum modeling and molecular dynamics simulation of torsional vibration of carbon nanotubes, IEEE Transactions on Nanotechnology 11 (2012) 34–43.

[22] S. Narendar, D. R. Mahapatra, S. Gopalakrishnan, Prediction of nonlocal scaling parameter for armchair and zigzag single-walled carbon nanotubes based on molecular structural mechanics, nonlocal elasticity and wave propagation, International Journal of Engineering Science 49 (2011) 509–522.

[23] A. C. Eringen, Nonlocal Continuum Field Theories, Springer-Verlag, 2002.

[24] E. Benvenuti, A. Simone, One-dimensional nonlocal and gradient elasticity: Closed-form solution and size effect, Mechanics Research Communications 48 (2013) 46–51.

[25] R. C. Picu, The Peierls stress in non-local elasticity, Journal of the Mechanics and Physics of Solids 50 (2002) 717–735.

[26] D. C. Rapaport, The art of molecular dynamics simulation, Cambridge University Press, 2004.

[27] J. Nocedal, S. J. Wright, Numerical optimization, Springer, 2006.

[28] E. G. Lewars, Computational chemistry: introduction to the theory and applications of molecular and quantum mechanics, Springer, 2010.

[29] C. Q. Ru, Effect of van der waals forces on axial buckling of a double-walled carbon nanotube, Journal of Applied Physics 87 (2000) 7227–7231.

[30] A. L. Kalamkarov, A. V. Georgiades, S. K. Rokkam, V. P. Veedu, M. N. Ghasemi-Nejhad, Analytical and numerical techniques to predict carbon nanotubes properties, International Journal of Solids and Structures 43 (2006) 6832–6854.

[31] J. Kołoczek, Y.-K. Kwon, A. Burian, Characterization of spatial correlations in carbon nanotubes-modelling studies, Journal of Alloys and Compounds 328 (2001) 222–225.

[32] S. Reich, C. Thomsen, J. Maultzsch, Carbon nanotubes: basic concepts and physical properties, John Wiley & Sons, 2008.

[33] Y. Huang, J. Wu, K. C. Hwang, Thickness of graphene and single-wall carbon nanotubes, Physical Review B 74 (2006) 245413.

[34] B. G. Demczyk, Y. M. Wang, J. Cumings, M. Hetman, W. Han, A. Zettl, R. O. Ritchie, Direct mechanical measurement of the tensile strength and elastic modulus of multiwalled carbon nanotubes, Materials Science and Engineering A 334 (2002) 173–178.

[35] G. V. Lier, C. V. Alsenoy, V. V. Doren, P. Geerlings, Ab initio study of the elastic properties of single-walled carbon nanotubes and graphene, Chemical Physics Letters 326 (2000) 181–185.

[36] B. WenXing, Z. ChangChun, C. WanZhao, Simulation of Young's modulus of single-walled carbon nanotubes by molecular dynamics, Physica B 352 (2004) 156–153.

[37] M. Meo, M. Rossi, Prediction of Youngs modulus of single wall carbon nanotubes by molecular-mechanics based finite element modelling, Composites Science and Technology 66 (2006) 1597–1605.

[38] T. Chang, H. Gao, Size-dependent elastic properties of a single-walled carbon nanotube via a molecular mechanics model, Journal of the Mechanics and Physics of Solids 51 (2003) 1059–1074.

[39] J. R. Xiao, B. A. Gama, J. W. G. Jr., An analytical molecular structural mechanics model for the mechanical properties of carbon nanotubes, International Journal of Solids and Structures 42 (2005) 3075–3092.

[40] H. Tashakori, B. Khoshnevisan, F. Kanjuri, Ab initio systematic study of chirality effects on phonon spectra, mechanical and thermal properties of narrow single walled carbon nanotubes, Computational Materials Science 83 (2014) 16–21.

[41] F. Shimizu, S. Ogata, J. Li, Theory of shear banding in metallic glasses and molecular dynamics calculations, Materials Transactions 48 (2007) 2923–2927.

[42] J. Y. Huang, S. Chen, Z. F. Ren, Z. Q. Wang, D. Wang, M. Vaziri, Z. Suo, G. Chen, M. S. Dresselhaus, Kink formation and motion in carbon nanotubes at high temperatures, Physical Review Letters 97 (2006) 075501.

[43] K. Chandraseker, S. Mukherjee, Coupling of extension and twist in single-walled carbon nanotubes, Journal of Apllied Mechanics 73 (2006) 315–326.

[44] J. Wu, K. C. Hwang, Y. Huang, An atomistic-based finite-deformation shell theory for single-wall carbon nanotubes, Journal of the Mechanics and Physics of Solids 56 (2008) 279–292.

[45] J. Peng, J. Wu, K. C. Hwang, J. Song, Y. Huang, Can a single-wall carbon nanotube be modeled as a thin shell?, Journal of the Mechanics and Physics of Solids 56 (2008) 2213–2224.

[46] C. Q. Ru, Chirality-dependent mechanical behavior of carbon nanotubes based on an anisotropic elastic shell model, Mathematics and Mechanics of Solids 14 (2008) 88–101.

[47] C. Bajaj, A. Favata, P. Podio-Guidugli, On a nanoscopically-informed shell theory of single-wall carbon nanotubes, European Journal of Mechanics A/Solids 42 (2013) 137–157.

[48] C. Q. Ru, Effective bending stiffness of carbon nanotubes, Physical Review B 62 (2000) 9973.

[49] C. Y. Wang, C. Ru, A. Mioduchowski, Axially compressed buckling of pressured multiwall carbon nanotubes, International Journal of Solids and Structures 40 (2003) 3893–3911.

[50] A. Pantano, D. M. Parks, M. C. Boyce, Mechanics of deformation of single- and multi-wall carbon nanotubes, Journal of the Mechanics and Physics of Solids 52 (2004) 789–821.

[51] L. Shen, J. Li, Transversely isotropic elastic properties of single-walled carbon nanotubes, Physical Review B 69 (2004) 045414.

[52] L. Wang, Q. Zheng, J. Z. Liu, Q. Jiang, Size dependence of the thin-shell model for carbon nanotubes, Physical Review Letters 95 (2005) 105501.

[53] J. Geng, T. Chang, Non linear stick-spiral model for predicting mechanical behavior of single-walled carbon nanotubes, Physical Review B 74 (2006) 245428.

[54] S. Plimpton, Fast parallel algorithms for short-range molecular dynamics, Journal of computational physics 117 (1995) 1–19.

[55] M. Malagù, E. Benvenuti, C. A. Duarte, A. Simone, One-dimensional nonlocal and gradient elasticity: Assessment of high order approximation schemes, Computer Methods in Applied Mechanics and Engineering 275 (2014) 138–158.

[56] T. J. R. Hughes, J. A. Cottrell, Y. Bazilevs, Isogeometric analysis: CAD, finite elements, NURBS, exact geometry and mesh refinement, Computer Methods in Applied Mechanics and Engineering 194 (2005) 4135–4195.